Xu, X.; Wang, W.; Nie , Y.; Kratz, K.; Ma , N.; Lendlein, A.:
Fine-tuning of Rat Mesenchymal Stem Cell Senescence via Microtopography of Polymeric Substrates.
In: MRS Advances . Vol. 5 (2020) 12 - 13, 643 - 653.
First published online by Cambridge University Press: 02.12.2019

DOI: 10.1557/adv.2019.446
https://dx.doi.org/10.1557/adv.2019.446

Fine-tuning of Rat Mesenchymal Stem Cell Senescence via Microtopography of Polymeric Substrates

Xun Xu[1], Weiwei Wang[1], Yan Nie[1,2], Karl Kratz[1], Nan Ma[1,3] and Andreas Lendlein[1,2,3]

[1] Institute of Biomaterial Science and Berlin-Brandenburg Center for Regenerative Therapies, Helmholtz-Zentrum Geesthacht, 14513 Teltow, Germany
[2] Institute of Chemistry, University of Potsdam, 14476 Potsdam, Germany
[3] Institute of Chemistry and Biochemistry, Freie Universität Berlin, 14195 Berlin, Germany

ABSTRACT

Cellular senescence, a driver of aging and age-related diseases, is a stable state found in metabolically active cells characterized by irreversible cell growth arrest and dramatic changes in metabolism, gene expression and secretome profile. Endogenous regeneration efficacy of mesenchymal stem cells (MSCs) could be attenuated due to senescence. MSCs can be modulated by not only biochemical signals but also by physical cues such as substrate topography. To provide a cell culture substrate that can prevent MSC senescence over an extended period of in vitro cultivation, here, the cell- and immunocompatible poly(ether imide) (PEI) substrate was used. Two distinct levels of roughness were created on the bottom surfaces of PEI inserts via injection molding: Low-R (similar to the thickness of attached single MSC, Rq: 3.9 ± 0.2 µm) and High-R (larger than single MSC thickness. Rq: 22.7 ± 0.8 µm). Cell expansion, lysosomal enzymatic activity, apoptosis and paracrine effects of senescent MSCs were examined by cell counting, detection of senescence-associated β-galactosidase (SA β-gal), Caspase 3/7, and CFSE labeling. MSCs showed high cell viability and similar spindle-shaped morphology on all investigated surfaces. Cells on Low-R presented the highest expansion (80000 ± 1805 cells), as compared to cells on smooth PEI and High-R. The low apoptosis level (0.08 vs 0.12 from smooth PEI) and senescence ratio (35% vs. 54% from smooth PEI) were observed in MSCs cultured on Low-R. The secretome from Low-R effectively prevents senescence and supports the proliferation of neighboring cells (1.5-fold faster) as compared to the smooth PEI secretome. In summary, the Low-R PEI provided a superior surface environment for MSCs, which promoted proliferation, inhibited apoptosis and senescence, and effectively influenced the proliferation of neighboring cells via their paracrine effect. Such microroughness can be considered as a key parameter for improving the therapeutic potential of endogenous regeneration, anti-organismal aging and anti-age-related pathologies via directly promoting cell growth and modulating paracrine effects of the senescence associated secretome.

INTRODUCTION

Cells that continually experience extrinsic or intrinsic stresses including chronic infection [1], nutrient starvation [2], abuse in alcohol consumption [3], high glucose [4], ultraviolet radiation [5] and oxidative stress [6], can enter into a state of permanent cell growth arrest that is termed cellular senescence. Apoptosis and senescence are two main processes that prevent the emergence of transformed cells in response to the stresses. Unlike cell apoptosis, which quickly eliminates the damaged or stressed cells, the senescent cells remain alive and highly secretory for an extended period of time [7]. The accumulation of senescent cells can be observed in aging and age-related pathologies [8]. Thus, identifying senescent cells has an important diagnostic and therapeutic potential.
There are several distinguishing characteristics of senescence such as growth arrest, altered cell morphology, resistance of apoptosis, secretion of senescence-associated secretory phenotype and enhanced enzymatic activity of the lysosomal hydrolase senescence-associated β-galactosidase (SA β-gal) [8]. During senescence, the original spindle-shaped cells can become multinucleated, flattened (fried egg-like) or remain spindle-shaped, which is highly dependent on the sources and types of triggers [9, 10]. Several cell types acquire resistance to apoptosis when they become senescent, while some are capable of undergoing apoptosis after senescence [7]. Still, the factor that determines whether cells undergo senescence or apoptosis remains elusive. Senescent cells release a variety of pro-inflammatory cytokines, growth factors and extracellular matrix-degrading proteases. Consequently, the senescence-associated cell growth arrest can be reinforced and senescence of the neighboring cells can be induced and recruited in a paracrine manner [11]. None of these aforementioned markers is sufficient on its own for identifying senescent cells. So far, besides the growth arrest, the most distinctive measurable feature of senescent cells is SA β-gal, which is derived from the lysosome and highly associated with the enhanced lysosomal biogenesis during the process of cellular senescence [12].

Mesenchymal stem cells (MSCs) offer tremendous potential for endogenous regeneration due to their differentiation potential, paracrine effect, and immunoregulatory function [13]. There is a broad anatomical distribution of MSCs, however, less than 0.01% MSCs can be isolated from their origins [14]. Substantial amounts of MSCs are required to achieve an effective therapy (from 100 million to 10 billion cells), which means approximately 17 doublings of 100 thousand MSCs have to be completed prior to cell implantation [4, 15]. Therefore, *in vitro* expansion of MSCs is inevitable. However, when the primary cell culture reaches the upper limit of cell population doubling level (20 to 40 depending on donor age), like other somatic cells, MSCs can undergo cellular senescence and gradually lose their ability to replicate [16].

Eliminating senescent cells and attenuating the production of senescence-associated secretome have emerged as attractive therapeutic strategies. Several attempts to prevent, retard or rescue cells from senescence have been reported. For instance, the initial selection of adjuvant donor and cell source [17], cryopreservation of early passage of primary isolated cells [18], introduction of the catalytic subunit of telomerase to cells by genetic engineering [19], and application of medium supplement including exogenous growth factors (FGF-2, PDGF and EGF) [20, 21]. Nowadays, growing evidence suggested that not only chemical composition [22, 23], but also physical features such as hydrophilicity, fluidity and stiffness of the surface could modulate senescence [24-26]. MSCs are highly sensitive to the physical properties of their microenvironment. Accumulated evidence indicates that the secretion and proliferation capacity of MSCs can be altered via geometry [27], stiffness [28] and topography of culture substrates [29]. Therefore, the demand for a surface with appropriate topology that supports high passage MSC expansion and avoids cellular senescence has arisen.

In this study, we hypothesized that the senescence stage of MSCs can be avoided by providing topographical cues of culture substrates. Poly(ether imide) (PEI) is a widely used and commercially available biocompatible polymer for hematological, chondrogenesis, cardiomyogenesis and immunological research due to its thermal stability, dielectric, mechanical and chemical strength, immune privilege as well as tailoring properties [30-34]. A smooth surface and surfaces with two levels of roughness were created at the bottom of PEI cups via injection molding: a smooth surface (Rq: 0.2 ± 0.1 µm); a surface with low roughness (Low-R, corresponding to the thickness of single attached MSC, Rq: 3.9 ± 0.2 µm); and a surface with high roughness (High-R, surpassing the thickness of single MSC, Rq: 22.7 ± 0.8 µm). Prior to cell seeding, rat bone marrow-derived MSCs were pre-cultivated until proliferation arrest was reached (passage 10). It is necessary to track the MSC expansion, SA β-gal activity and the senescence-associated secretome following growth arrest, enzymatic activity of lysosome and paracrine effect are the key consequences of senescence and the signs of senescence level [35]. Here, we investigated the senescence-associated changes in comparison to the standard smooth culture substrate tissue culture plate (TCP) with regard to cell shape, viability, apoptosis level, SA β-gal activity, cell expansion, and paracrine effect on cell division (Figure 1A and B).

EXPERIMENTAL DETAILS

The fabrication, characterization and sterilization of microstructured PEI substrates were described in a previous study [33]. In brief, PEI with a number average molecular weight (M_n) of 18000 g/mol (General Electric, USA) was used for fabrication. Three differently structured cylinders (a cylinder with a polished surface, and two cylinders with microstructured surfaces according to the standard of German Institute for Standardization (DIN 16747: 1981-05), M30 (Low-R) and M45 (High-R)) were utilized to create the surfaces. The roughness profile was analyzed using an optical profilometer equipped with a CWL 300 chromatic white-light sensor (Fries Research & Technologie GmbH, Germany). Each analysis was performed in an area of 7 x 7 mm^2 (4000 lines per image, 250 dots per line, 300 Hz). All PEI substrates were sterilized via steam sterilization (121°C, 200 kPa, 20 minutes) using a Systec Autoclave D-65 (Systec GmbH, Germany) prior to biological evaluation. TCP (TPP Techno Plastic Products AG, Germany) was used as a standard smooth culture substrate. Rat bone marrow-derived MSCs were kindly provided by Dr. Jun Li (University of Rostock, Germany. Approval number: LALLF M-V/TSD/7221.3-2.3-019/07), which were isolated from bone marrow of Lewis rat as described previously [36]. Cells were cultured in DMEM medium containing 10 vol% fetal bovine serum and were seeded as single cells on the microstructured substrates and in the upper wells of transwell system (0.4 µm pores) with a density of 1×10^4 cells/cm^2. The cells from passage 10, which reached proliferation arrest (defined as more than 80% cells being blocked at G0/G1 phase, as determined by flow cytometry) were used for the following experiments.

At day 5, viable cells were detected using fluorescein diacetate (FDA, 25 µg/mL) and necrotic cells were stained with propidium iodide (PI, 2 µg/mL) (Sigma Aldrich Chemie GmbH, Germany). Confocal microscopy (LSM 780, Carl Zeiss GmbH, Germany) was utilized to observe the stained cells. Senescence Cells Histochemical Staining Kit (Sigma Aldrich Chemie GmbH, Germany) was applied to identify senescent cells via detecting SA β-gal activity at pH 6. The senescence ratio was expressed as the percentage of the senescent cells out of total cells. ApoLive-Glo Multiplex Assay Kit (Promega GmbH, Germany) was used for determination of apoptotic MSCs. Cells grown on PEI substrates and TCP for 20 days were harvested, the relative fluorescence units (RFU) from

total cells were measured at 400 nm (excitation) /505 nm (emission) and the Caspase-3/7 activation was determined by measuring the relative light units (RLU) of the luminescence using a Tecan Infinite 200 PRO microplate reader (Tecan Deutschland GmbH, Germany). Cell expansion was measured using Cell Counting kit-8 (Sigma Aldrich Chemie GmbH, Germany), the absorbance was detected at 490 nm (reference: 650 nm) by using a microplate reader (Tecan Deutschland GmbH, Germany). Cell division was assessed by quantifying the reduction of mean fluorescence intensity (MFI) of CFSE via flow cytometry (MACSQuant Analyzer, Miltenyi Biotec, Germany). In brief, cells were pre-labelled with 20 µM CFSE and then cultured for 20 days. The transwell system was used to segregate CFSE-labelled cells in upper wells with 0.4 µm pores and cells in contact with PEI substrates or TCP.

Statistical analysis was performed using one-way ANOVA for single factor (microroughness) analysis and two-way ANOVA (for two factors: time and microroughness) with post-hoc Tukey HSD test, and a p value < 0.05 was considered to be statistically significant. All data were from at least three independent experiments and presented as mean ± standard deviation.

RESULTS AND DISCUSSION

Microscale roughness does not affect MSC morphology and viability

The MSC fate and cellular functions can be modulated by multiple topographical cues of cell culture substrates. This external physical information needs to be sensed, translated and transmitted as readable biological signals by MSCs intracellularly. In response to this process, a cytoskeletal reorganization or a visible morphological change may occur [27, 37]. To determine the shape change and viability of MSCs growing on smooth PEI and surfaces comprising different microroughness levels, living cells were stained with FDA (green) and dead cells were discriminated by labelling with PI (red) at day 5 of cultivation. The typical spindle shape and a low death level of MSCs grown on all PEI surfaces were observed. Cells grown on PEI surfaces did not show remarkable difference to TCP with respect to morphology and cell viability. Therefore, cell shape and viability was not altered by the microroughness of PEI substrates according to the confocal imaging analysis of FDA/PI staining (Figure 1C).

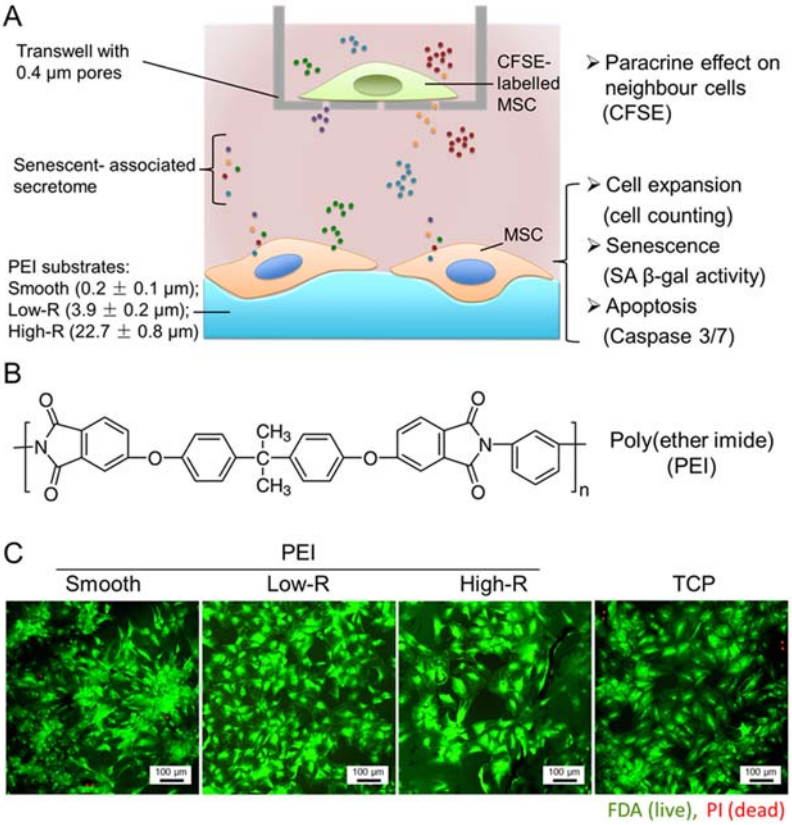

Figure 1. Experimental design and MSC viability assay. (A) Schematic illustration of the experimental setting. (B) Chemical structure of PEI. (C) Representative fluorescent images of MSCs counterstained with FDA (green, indicating living cells) and PI (red, indicating dead cells). Cells were growing on PEI surfaces comprising different microroughness levels as well as on TCP surface for 5 days. Scale bar =100 µm.

Microscale roughness supports cell expansion

In spite of a larger contact area provided by a rough surface, in our study, a similar initial cell adhesion rate was found in cells grown on both smooth PEI and rough Low-R surfaces. This is in contrast to a previous study, which demonstrated that MSCs exhibited a lower attachment on a titanium surface with a roughness relevant to the cell size [38]. The possible reasons for this discrepancy might be the distinct surface chemistry as well as the different protein adsorption levels of the materials. Starting from day 5, MSCs grown on TCP showed significantly higher cell numbers than that on smooth PEI surfaces. The chemical properties and the stiffness of polymer substrates could affect various MSC behaviors including cell attachment, morphology and cell cycle progression [39, 40]. Therefore, both of the chemical and mechanical differences between PEI and TCP might result in the different proliferation rate. At day 10, cells grown on Low-R PEI surface presented the highest cell number (80000 ± 1805 cells), as compared to cells on smooth PEI (65000 ± 2173 cells) and High-R (73705 ± 3044 cells) (Figure 2). This might be

attributed to the highest and higher apoptosis and senescence level of cells on smooth and High-R PEI surfaces (Figure 3 and 4). This observation is in agreement with the finding that there was a negative correlation of cell expansion number with cell senescence and apoptosis levels [41]. In addition, by using two-way ANOVA statistical analysis, we found that the culture time could further influence the effect of microroughness on cell expansion (Figure 2).

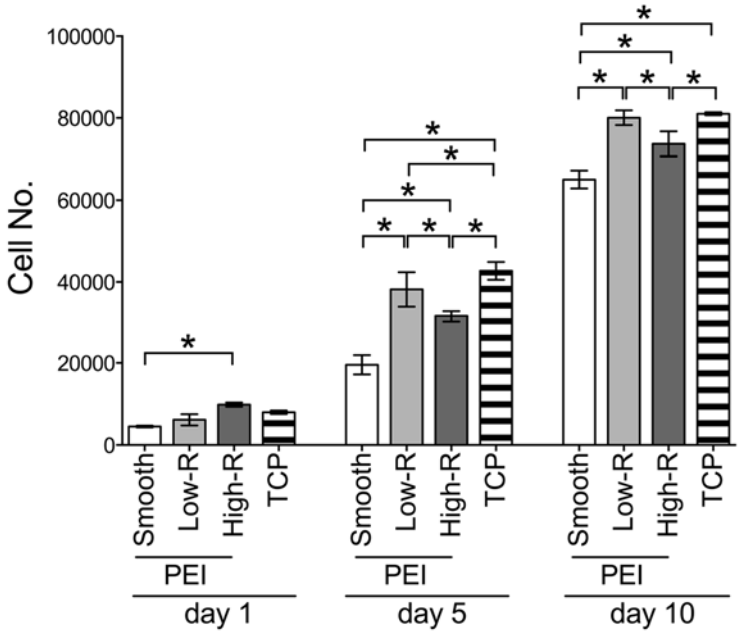

Figure 2. Expansion of MSCs cultured on PEI surfaces comprising smooth and two different levels of microroughnesses as well as TCP surface at indicated time points (Mean ± SD, n=3, *p<0.05, by two-way ANOVA with post-hoc Tukey HSD test, Interaction: microroughness vs. time, F = 17.87, *p < 0.05, effect of microroughness, F = 45.41, *p < 0.05, effect of time, F = 2618, *p < 0.05).

Microscale roughness prevents MSC senescence

To access the senescence level, we analyzed SA β-gal activity in MSCs cultured on PEI surfaces with distinct microroughness for 20 days. We found that the percentage of SA β-gal positive MSCs on the Low-R PEI surface was lower (35 ± 4% decreased) compared to those on the smooth PEI surface (Figure 3). These results suggested that in contrast to the smooth surface, PEI substrate with a microroughness level fitting the single cell thickness (Low-R) was capable to prevent cellular senescence of MSCs and maintain the SA β-gal marker at the lowest level after an extended period of cell culture.

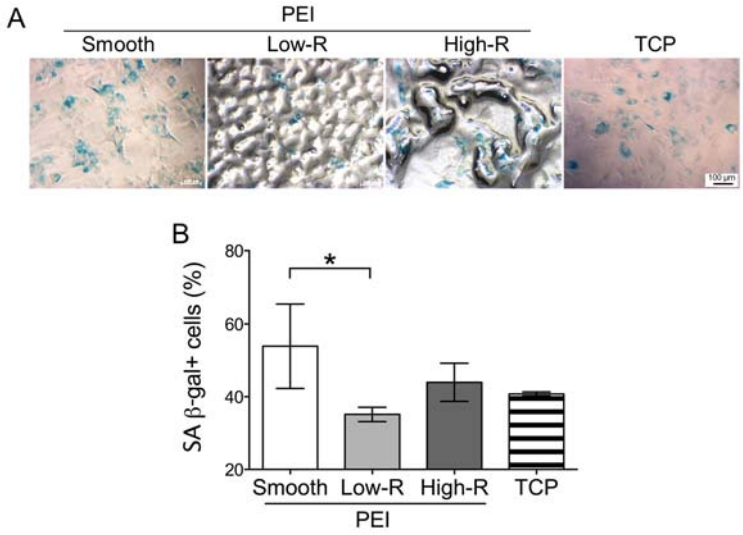

Figure 3. Influence of microscale roughness on cellular senescence of MSCs. (A) Representative images of SA β-gal staining (cyan) of cells on smooth, Low-R, High-R of PEI and smooth TCP at pH 6. Scale bar =100 μm. (B) The number of SA β-gal-positive cells and total cells were counted based on four randomly selected images. The result was expressed as the percentage of the SA β-gal-positive senescent cells out of total cells (Mean ± SD, n=4, *p<0.05, by one-way ANOVA with post-hoc Tukey HSD test).

Microscale roughness modulates MSC apoptosis level

Here, the Caspase-3/7 positive cells existing on PEI and TCP surfaces were monitored for an indicated time period. At day 1, the apoptosis levels of MSCs on both rough surfaces (Low-R and High-R) were significantly lower compared to smooth surfaces (smooth PEI and TCP). At day 5, the lowest apoptosis level was preserved in MSCs on Low-R surface. After a 10-day cultivation, the apoptosis levels of MSCs decreased dramatically and there were no significant differences in apoptosis levels between all examined groups (Figure 4). As an acute response to environmental stimuli, apoptosis-related biochemical events appeared within 24 hours [42, 43], longer exposure time (more than 10 days) might be required when the culture condition was altered [44]. In our study, the peak level of apoptosis was detected within 5 days, and PEI substrates with appropriate microroughness Low-R could efficiently down-regulate cell apoptosis.

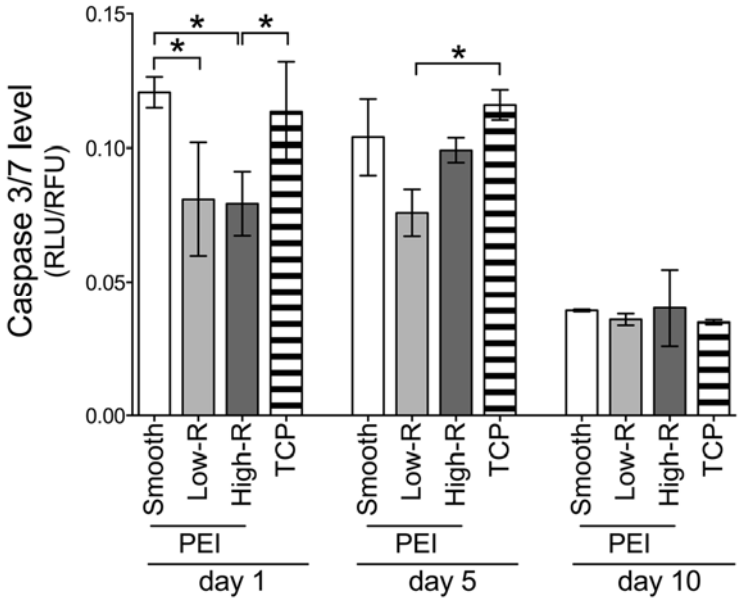

Figure 4. Apoptosis levels of MSCs grown on PEI inserts comprising different microroughness and on TCP were measured at the time points indicated. RLU value of Caspase 3/7 active apoptotic cells was normalized with RFU value of total cells (Mean ± SD, n=3, *p<0.05, by two-way ANOVA with post-hoc Tukey HSD test, Interaction: microroughness vs. time, F = 3.705, p = 0.1163, effect of microroughness, F = 31.21, *p < 0.05, effect of time, F = 17.29, p = 0.0547).

Microscale roughness promotes cell division via paracrine signaling

The composition of the senescence-associated secretome is highly dynamic. To minimize the interference on paracrine effects during manual collection of conditioned medium, a transwell system with 0.4 μm pores at the bottom surface was introduced. On one hand, it supported the anchorage-dependent cell attachment and growth. On the other hand, only the secretome produced by cells could freely diffuse to reach the target cells, while cells inside and outside the transwell were unable to penetrate through the pores. The target cells were cultured in the transwell (upper well) and prior to cell seeding, they were stained with the non-fluorescent dye CFSE, which can be cleaved by intracellular esterase and couples to amines to irreversibly form fluorescent conjugates. The CFSE-conjugates are distributed equally between daughter cells when the cell proliferates and divides. Therefore, CFSE labeling was applied to monitor the target MSC growth.

MSCs directly in contact with the PEI surfaces comprising different levels of microroughness or on TCP were co-cultured with the CFSE-labelled cells (upper well) for 20 days (Figure 1A). Approximately, only half of accumulated CFSE signal shown from smooth PEI co-cultures was detected in the MSCs from Low-R co-cultures. In other words, cell proliferation rate of target cells receiving secretomes from MSCs grown on Low-R surface was two-fold higher than that on smooth PEI surface. Notably, the proliferation

rates of cells in Low-R and High-R group were significantly higher than both smooth groups (smooth PEI and TCP), indicating that the microscale roughness could effectively retard the paracrine mediated cellular senescence (Figure 5A and B).

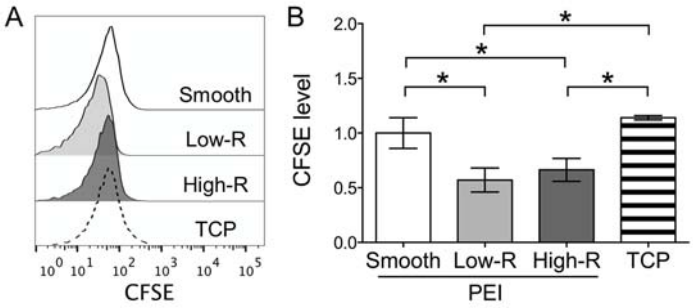

Figure 5. Effect of paracrine on MSC proliferation. (A) Representative histogram of CFSE peak of cells grown in the upper wells of transwells (lacking of direct contact to PEI surfaces) co-cultured with cells attached on PEI surfaces with different roughness levels for 20 days. (B) Quantitative analysis of the CFSE level of MSCs grown in the upper wells of transwells. Low MFI level indicate high proliferation rates. CFSE level of cells in the group of smooth PEI was set as 1 (Mean ± SD, n=3, * $p<0.05$, by one-way ANOVA with post-hoc Tukey HSD test).

CONCLUSIONS

Rat bone marrow-derived MSCs showed similar morphology on all PEI surfaces with distinct microroughness levels, which also exhibited a remarkably high cell viability. This qualifies PEI as a suitable cell culture substrate material. Nevertheless, low senescent and apoptosis levels were both retained in MSCs grown on PEI substrates with an appropriate microroughness fitting the single attached MSC thickness (Low-R). Additionally, the elevated cell expansion (15000 cells more at day 10) and accelarated paracrine mediated cell division (2-fold at day 20) were observed in the group of Low-R. These observations provided fundamental blocks to achieve a meaningful number of healthy stem cells for therapeutic applications without chemical and genetic manipulation. These findings also highlighted the capability of preventing the cellular senescence of primary stem cells and improving the quality and therapeutic potential of stem cells via modification of the topographical microstuctures of *in vitro* cell culture surfaces. Considering the better cell expansion observed at smooth TCP in comparison of smooth PEI, TCP surface with microroughness at the single cell level (Low-R) can be created and utilized for the future applications to further improve the effectiveness of suppressing stem cell cellular senescence.

ACKNOWLEDGMENTS

This work was financially supported by the Helmholtz-Association of German Research Centers (through program-oriented funding, and through the Helmholtz Graduate School of Macromolecular Bioscience [MacroBio], grant no. VH-GS-503, the Helmholtz Cross Program Initiative "Technology and Medicine - Adaptive Systems", Helmholtz Virtual Institute, Multifunctional Biomaterials for Medicine (grant no. VH-VI-423)) and the

Federal Ministry of Education and Research, Germany, for funding through the Program Health Research (grant no. 13GW0098, and project number 0315696A "Poly4BioBB"). The authors acknowledge Robert Bendisch and Mario Rettschlag for the preparation of sterilized PEI inserts and Manuela Keller for technical support.

REFERENCES

1. M. O. Aguilera, L. R. Delgui, P. S. Romano and M. I. Colombo, *Cells* **7** (10), 162 (2018).
2. B. Carroll and V. I. Korolchuk, *FEBS J.* **285** (11), 1948-1958 (2018).
3. X. Chen, M. Li, J. Yan, T. Liu, G. Pan, H. Yang, M. Pei and F. He, *Alcohol Alcohol.* **52** (3), 289-297 (2017).
4. D. Zhang, H. Lu, Z. Chen, Y. Wang, J. Lin, S. Xu, C. Zhang, B. Wang, Z. Yuan, X. Feng, X. Jiang and J. Pan, *Mol. Med. Rep.* **16** (2), 1685-1690 (2017).
5. F. Debacq-Chainiaux, C. Borlon, T. Pascal, V. Royer, F. Eliaers, N. Ninane, G. Carrard, B. Friguet, F. de Longueville, S. Boffe, J. Remacle and O. Toussaint, *J. Cell Sci.* **118** (Pt 4), 743-758 (2005).
6. A. Brandl, M. Meyer, V. Bechmann, M. Nerlich and P. Angele, *Exp. Cell Res.* **317** (11), 1541-1547 (2011).
7. A. Seluanov, V. Gorbunova, A. Falcovitz, A. Sigal, M. Milyavsky, I. Zurer, G. Shohat, N. Goldfinger and V. Rotter, *Mol. Cell. Biol.* **21** (5), 1552-1564 (2001).
8. B. G. Childs, M. Durik, D. J. Baker and J. M. van Deursen, *Nat. Med.* **21** (12), 1424-1435 (2015).
9. O. Moujaber, F. Fishbein, N. Omran, Y. Liang, I. Colmegna, J. F. Presley and U. Stochaj, *Cell. Mol. Life Sci.* **76** (6), 1169-1183 (2019).
10. T. Kuilman, C. Michaloglou, W. J. Mooi and D. S. Peeper, *Genes Dev.* **24** (22), 2463-2479 (2010).
11. J. C. Acosta, A. Banito, T. Wuestefeld, A. Georgilis, P. Janich, J. P. Morton, D. Athineos, T. W. Kang, F. Lasitschka, M. Andrulis, G. Pascual, K. J. Morris, S. Khan, H. Jin, G. Dharmalingam, A. P. Snijders, T. Carroll, D. Capper, C. Pritchard, G. J. Inman, T. Longerich, O. J. Sansom, S. A. Benitah, L. Zender and J. Gil, *Nat. Cel. Biol.* **15** (8), 978-990 (2013).
12. G. P. Dimri, X. Lee, G. Basile, M. Acosta, G. Scott, C. Roskelley, E. E. Medrano, M. Linskens, I. Rubelj, O. Pereira-Smith and et al., *Proc. Natl. Acad. Sci. U. S. A.* **92** (20), 9363-9367 (1995).
13. C. Brown, C. McKee, S. Bakshi, K. Walker, E. Hakman, S. Halassy, D. Svinarich, R. Dodds, C. K. Govind and G. R. Chaudhry, *J. Tissue Eng. Regener. Med.* **13** (9), 1738-1755 (2019).
14. S. A. Wexler, C. Donaldson, P. Denning-Kendall, C. Rice, B. Bradley and J. M. Hows, *Br. J. Haematol.* **121** (2), 368-374 (2003).
15. Y. K. Yang, *Regener. Ther.* **9**, 120-122 (2018).
16. E. S. Hwang, *Cell. Mol. Life Sci.* **71** (21), 4207-4219 (2014).
17. A. Stolzing, E. Jones, D. McGonagle and A. Scutt, *Mech. Ageing Dev.* **129** (3), 163-173 (2008).
18. L. Hayflick, *Exp. Gerontol.* **24** (5-6), 355-365 (1989).
19. J. L. Simonsen, C. Rosada, N. Serakinci, J. Justesen, K. Stenderup, S. I. Rattan, T. G. Jensen and M. Kassem, *Nat. Biotechnol.* **20** (6), 592-596 (2002).
20. B. Gharibi and F. J. Hughes, *Stem Cells Transl. Med.* **1** (11), 771-782 (2012).
21. A. Blazquez-Prunera, J. M. Diez, R. Gajardo and S. Grancha, *Stem Cell Res. Ther.* **8** (1), 103 (2017).
22. J. Zou, W. Wang, K. Kratz, X. Xu, Y. Nie, N. Ma and A. Lendlein, *Clin. Hemorheol. Microcirc.* **70** (4), 573-583 (2018).
23. S. H. Kim, B. M. Lee, S. K. Min, S. U. Song, J. H. Cho, K. Cho and H. S. Shin, *Colloids Surf., B* **90**, 36-40 (2012).
24. P. J. Lou, M. Y. Chiu, C. C. Chou, B. W. Liao and T. H. Young, *Biomaterials* **31** (7), 1568-1577 (2010).
25. S. S. Mano, K. Uto and M. Ebara, *Theranostics* **7** (19), 4658-4670 (2017).
26. S. K. Kureel, P. Mogha, A. Khadpekar, V. Kumar, R. Joshi, S. Das, J. Bellare and A. Majumder, *Biol. Open* **8** (4), bio039453 (2019).
27. X. Xu, W. Wang, K. Kratz, L. Fang, Z. Li, A. Kurtz, N. Ma and A. Lendlein, *Adv. Healthcare Mater.* **3** (12), 1991-2003 (2014).
28. N. Huebsch, P. R. Arany, A. S. Mao, D. Shvartsman, O. A. Ali, S. A. Bencherif, J. Rivera-Feliciano and D. J. Mooney, *Nat. Mater.* **9** (6), 518-526 (2010).
29. M. J. Dalby, N. Gadegaard, R. Tare, A. Andar, M. O. Riehle, P. Herzyk, C. D. Wilkinson and R. O. Oreffo, *Nat. Mater.* **6** (12), 997-1003 (2007).
30. M. Lange, S. Braune, K. Luetzow, K. Richau, N. Scharnagl, M. Weinhart, A. T. Neffe, F. Jung, R. Haag and A. Lendlein, *Macromol. Rapid Commun.* **33** (17), 1487-1492 (2012).

31. S. Braune, M. Lange, K. Richau, K. Lutzow, T. Weigel, F. Jung and A. Lendlein, *Clin. Hemorheol. Microcirc.* **46** (2-3), 239-250 (2010).
32. J. Konig, B. Kohl, K. Kratz, F. Jung, A. Lendlein, W. Ertel and G. Schulze-Tanzil, *Clin. Hemorheol. Microcirc.* **55** (4), 523-533 (2013).
33. X. Xu, W. Wang, Z. Li, K. Kratz, N. Ma and A. Lendlein, *Clin. Hemorheol. Microcirc.* **64** (3), 367-382 (2016).
34. T. Roch, A. Kruger, K. Kratz, N. Ma, F. Jung and A. Lendlein, *Clin. Hemorheol. Microcirc.* **52** (2-4), 375-389 (2012).
35. J. Campisi and F. d'Adda di Fagagna, *Nat. Rev. Mol. Cell Biol.* **8** (9), 729-740 (2007).
36. X. Xu, K. Kratz, W. Wang, Z. Li, T. Roch, F. Jung, A. Lendlein and N. Ma, *Clin. Hemorheol. Microcirc.* **55** (1), 143-156 (2013).
37. P. P. Provenzano and P. J. Keely, *J. Cell Sci.* **124** (Pt 8), 1195-1205 (2011).
38. M. Bigerelle, S. Giljean and K. Anselme, *Acta Biomater.* **7** (9), 3302-3311 (2011).
39. W. Wang, N. Ma, K. Kratz, X. Xu, Z. Li, T. Roch, K. Bieback, F. Jung and A. Lendlein, *Clin. Hemorheol. Microcirc.* **52** (2-4), 357-373 (2012).
40. W. Wang, X. Xu, Z. Li, K. Kratz, N. Ma and A. Lendlein, *Clin. Hemorheol. Microcirc.* **71** (2), 277-289 (2019).
41. K. Stenderup, J. Justesen, C. Clausen and M. Kassem, *Bone* **33** (6), 919-926 (2003).
42. M. Ramirez-Ortega, V. Maldonado-Lagunas, J. Melendez-Zajgla, J. F. Carrillo-Hernandez, G. Pastelin-Hernandez, O. Picazo-Picazo and G. Ceballos-Reyes, *Eur. J. Pharmacol.* **534** (1-3), 71-76 (2006).
43. S. Hartel, M. Zorn-Kruppa, S. Tykhonova, P. Alajuuma, M. Engelke and H. A. Diehl, *Cytometry, Part A* **55** (1), 15-23 (2003).
44. T. L. Riss and R. A. Moravec, *Assay Drug Dev. Technol.* **2** (1), 51-62 (2004).